Current Optics and Photonics
Vol. 2, No. 1, February 2018, pp. 47-52

ISSN: 2508-7266(Print) / ISSN: 2508-7274(Online)
DOI: https://doi.org/10.3807/COPP.2018.2.1.047

Negative-refraction Effect for Both TE and TM Polarizations in Two-dimensional Annular Photonic Crystals

Hong Wu[1]* and Feng Li[2,3]

[1]*School of Science, Nanjing University of Posts and Telecommunications, Nanjing, 210023, China*
[2]*IEK-5 Photovoltaik, Forschungszentrum Jülich, 52425 Jülich, Germany*
[3]*College of Chemistry and Materials Science, Jiangsu Key Laboratory of Biofunctional Materials, Nanjing Normal University, Nanjing 210023, China*

(Received November 15, 2017 : revised December 17, 2017 : accepted December 25, 2017)

We systematically investigated the negative-refraction effect for both TE and TM polarizations in annular photonic crystals. Since two polarization waves are excited in different bands, they result in different refractive angles, and so polarization beam splitters can be made of annular photonic crystals. It was found that, in comparison to normal square-lattice air-hole photonic crystals, annular photonic crystals have a much wider common frequency band between TE-1 and TM-2, which is quite beneficial to finding the overlap between the negative-refraction regions belonging to TE-1 and TM-2 respectively. Further analyses of equifrequency surfaces and the electric-field distribution of annular photonic crystals with different parameters have not only demonstrated how the filling factor of annular cells affects the formation of the common negative-refraction region between TE-1 and TM-2, but also revealed some ways to improve the performance of a polarization beam splitter based on the negative-refraction effect in an annular photonic crystal.

Keywords : Annular photonic crystals, Negative refraction, Polarization beam splitter
OCIS codes : (060.4510) Optical communication (130.3120) Integrated optics devices; (230.5298) Photonic crystals

I. INTRODUCTION

Since the pioneering works of Veselago [1] and Pendry [2] devoted to the imaging properties of a slab with simultaneous negative permittivity and permeability, there have been many efforts in the study of the negative-refraction effect at microwave frequencies in millimeter-patterned metallic materials [3, 4]. However, when infrared or visible light is considered, the limitations of the damping constants of metals must be faced. To overcome this difficulty at optical frequencies, the purely dielectric route, *i.e.* the photonic-crystal (PC) route, has attracted growing interest. A number of recent theoretical [5, 6] and experimental [7, 8] works have demonstrated that the negative-refraction effect is also possible in PCs. The physical principles that allow negative refraction in PCs arise from the dispersion characteristics of wave propagation in a periodic medium, which can be described well by analyzing the equifrequency surface (EFS) of the band structure. To realize the negative-refraction effect in a PC, the shape of the EFS at the operating frequency must be convex, which ensures that the direction of the group velocity of the refractive wave is on the same side of the normal direction as the incident wave. Using this general criterion, the negative-refraction region can usually be found for a normal two-dimensional (2D) PC (air-hole-type and pillar-type PCs) not only in the first band, but also in the second or higher bands.

It is well known that an electromagnetic wave can be decomposed into transverse magnetic (TM) polarization and transverse electric (TE) polarization for a 2D PC structure. However, investigations have shown that air-hole-type 2D

*Corresponding author: wuhong@njupt.edu.cn, ORCID 0000-0002-5773-7164
Color versions of one or more of the figures in this paper are available online.

PCs possess good negative behavior for the TE polarization, while a pillar-type 2D PC favors the TM polarization. Alternatively, many recent works have demonstrated that good negative behavior for both TE and TM polarizations can simultaneously be realized in annular PC (APC) structures. [9, 10] These novel systems have an unusual composition of annular dielectric rods in air or annular air voids in a dielectric background; this can be regarded as a combination of the two normal PC types [11-13]. Usually, researchers always focus their attention on the optical characteristics in the same band for the two polarizations. For instance, Zhang has indicated that absolute negative refraction can be realized in the first band of 2D composed PCs for both polarizations [9]. Jiang *et al*. have demonstrated the possibility of polarization-independent negative-refraction effect in the second band of APC structures [10].

Especially, in our previous work [14] the negative-refraction effect in APCs has been applied to design a novel kind of polarization beam splitter, when TE and TM polarizations were excited in different bands. Owing to the depressed band of the TM polarization induced by the inclusion of dielectric rods within the APC, a structure with some special filling factors will have a wide common frequency band between TE-1 and TM-2. Thus, the common negative-refraction region (CNRR) between TE-1 and TM-2 bands can be found. Unlike the polarization-independent effect occurring in the same band for two polarizations, as reported in Refs. [9] and [10], in the CNRR between TE-1 and TM-2, both polarization beams undergo negative refraction, but the corresponding refractive angles are different. As a result, the TE and TM polarization waves can be separated efficiently. Through an appropriate set of design parameters, the proposed polarization beam splitter can work within a wider normalized frequency range than a splitter based on negative-positive refraction [15, 16]. However, it remains unclear how the filling factor of the APC affects this polarization-beam-splitting effect. In this paper, we have systematically investigated the formation of CNRR between TE-1 and TM-2 in APCs, arranged as follows: In Sec. 2 we will present the main model and methods used in this study. For comparison, in Secs. 3 and 4 we will discuss the formation of CNRR between TE-1 and TM-2 in normal air-hole PCs and APCs respectively. Finally, a brief summary will be given in Sec. 5.

II. MODEL AND METHOD

As a model system, we consider a square-lattice APC, as illustrated in Fig. 1. The air rings with inner radius r and outer radius R are arranged in a dielectric material ($\varepsilon = 13$). The popular free software "MPB", which treats Maxwell's wave equation as the Hermitian eigenvalue problem with the plane-wave expansion (PWE) technique, is utilized to obtain the photonic band structures and EFSs

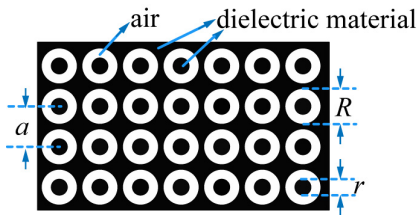

FIG. 1. Schematic diagram of the square-lattice APC.

of the PCs, and the finite-difference time-domain (FDTD) technique is adopted to simulate the energy distribution in the PCs and in free space.

III. THE FORMATION OF CNRR BETWEEN TE-1 AND TM-2 IN NORMAL PCs

Since the APCs studied in this paper are directly developed from the normal air-hole PCs, for comparison we begin the discussion by first studying the formation of CNRR between TE-1 and TM-2 in normal square-lattice air-hole PCs. By analyzing the EFSs for several frequencies, we have calculated the negative-refraction frequency range at TE-1 and TM-2 in several PCs with different values of air-hole radius. Figures 2(a)~2(c) show the dispersion diagrams when R is equal to $0.35a$, $0.47a$ and $0.5a$, and the calculated results are marked by blue and yellow strips for the TE and TM polarizations, respectively. Those marked regions have lower limits that are obtained by investigating the shape of EFSs, and upper limits that are directly found by computing the upper edges of TE-1 and TM-2. It is found that when R increases, the negative-refraction regions (NRRs) for both polarizations move to higher frequencies, and the separation of NRR-TE and NRR-TM is gradually suppressed. In particular, when R increases to $0.5a$, overlap occurs within the frequency range of 0.416-0.421 $2\pi c/a$, which means that the CNRR between TE-1 and TM-2 is available in the normal

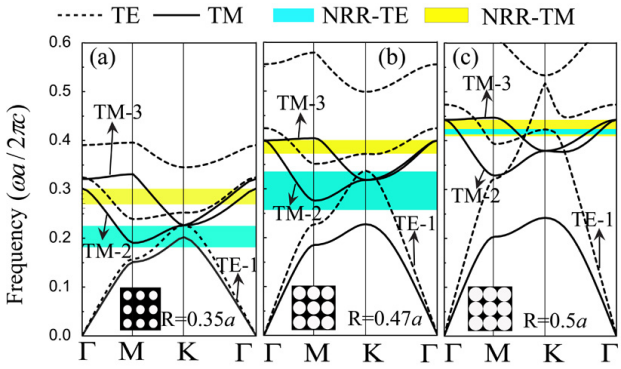

FIG. 2. The band structures of square-lattice air-hole PCs with different parameters. The blue and yellow strips correspond to the negative-refraction regions for TE and TM polarizations respectively.

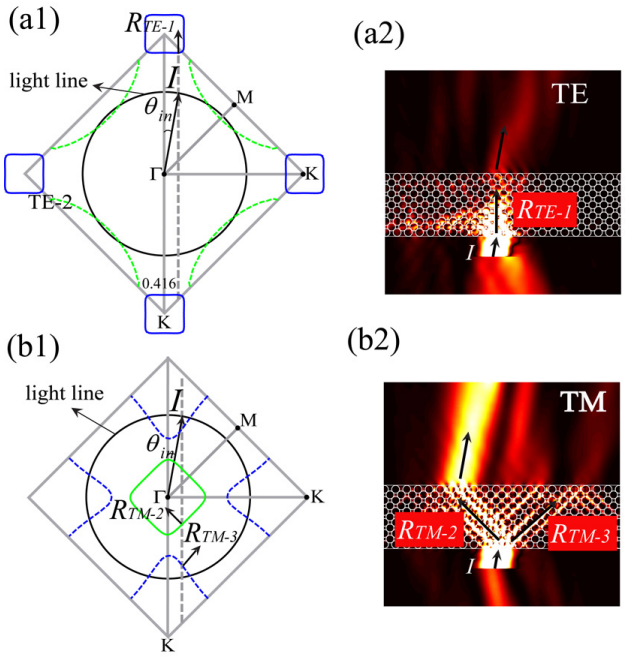

FIG. 3. The EFSs and electric-field distribution when a slit beam impinges upon the PC slab with angle of incidence θ_{in} = 10° for (a1, a2) TE and (b1, b2) TM. The radius of the air holes is 0.5a. R_{TE-1}, R_{TM-2}, and R_{TM-3} represent the negative-refracted beams inside the PC slab respectively.

square-lattice PC with the largest filling factor.

However, with further investigation of the band structures in Figs. 2(a)~2(c), we can see that as R increases, overlap of TM-2 and TM-3 in the Γ-K direction always exists. Additionally, when R increases from 0.35a to 0.47a we can see that the NRR-TE can be obviously widened by the enlarged TE-1 frequency range, which will be beneficial to obtaining a wide CNRR between TE-1 and TM-2. However, when R = 0.5a, the NRR-TE is unfortunately cut down by the shape distortion of TE-1 in the vicinity of the band edge, so the bandwidth of the CNRR shown in Fig. 2(c) is relative narrow. To check the negative-refraction effects, we chose the frequency 0.416 2πc/a as an example to perform numerical simulations in the air-hole PC with R = 0.5a. Figure 3 shows the calculated EFSs and the corresponding electric-field distribution when a slit beam impinges upon the PC slab with angle of incidence θ_{in} = 10°. For TE polarization, the EFS of TE-1 is convex around Γ (see Fig. 3(a1)). When the incident angle is 10°, one refracted beam (represented by R_{TE-1}) will be excited. However, since the frequency 0.416 2πc/a is very close to the edge of TE-1, an obviously low transmission prevents the formation of clearly negative refraction (see Fig. 3(a2)). Hence, to reduce reflection loss, shape distortion of the bands, which will cut down the NRR-TE, should be avoided.

On the other hand, for TM polarization we find that, owing to the overlap of TM-2 and TM-3, when the incident angle is 10° one incident wave will correspond to two refractive waves (represented by R_{TM-2} and R_{TM-3} in Figs. 3(b1) and 3(b2) respectively). This means that the PC cannot support single-beam negative refraction for TM polarization (see Fig. 3(b2)). Thus, to guarantee single-beam behavior, the CNRR should be modified by deleting the overlap region, which will be referred to as single-beam CNRR. This means it will be a tough task to find satisfactory dispersion characteristics for normal air-hole PCs, when only the radius of the air holes can be adjusted.

IV. THE FORMATION OF SINGLE-BEAM CNRR BETWEEN TE-1 AND TM-2 IN APCs

Now let us turn our attention to APCs. Apparently, compared to normal air-hole PCs, the extra dielectric cylinders centered in the air holes give us more freedom to adjust the band structures of APCs. To find possible structures of APCs with satisfactory dispersion relationships, it is necessary to investigate different values of the radii R and r.

For example, Fig. 4 presents the band structures of an APC (R = 0.47a) when different values of r are considered; the calculated single-beam NRRs (obtained by removing the overlapping regions in NRRs) are also marked in the

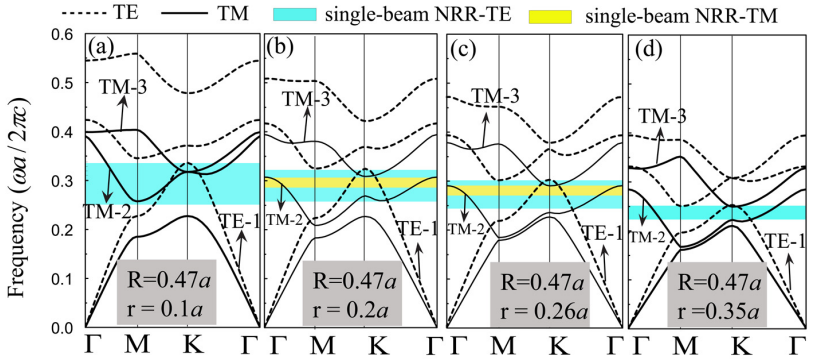

FIG. 4. The band structures of square-lattice APCs with different values of r when R = 0.47a. The blue and yellow strips correspond to the single-beam negative-refraction regions for TE and TM polarizations respectively.

figures. It is found that as r increases, the single-beam NRR-TE is gradually pulled down to lower frequencies, and the bandwidth is gradually reduced by the suppressed band structures. Different from the monotonic behavior of the single-beam NRR-TE, the single-beam NRR-TM experiences more complex properties, which should be investigated in detail as follows: When r increases from 0.1a to 0.2a, since the TM-2 band falls to a greater degree than the TM-3 band, the separation of these two bands is gradually enhanced. Particularly, when $r = 0.2a$ the single-beam NRR-TM is available within the frequency range of 0.277-0.304 $2\pi c/a$,. As r varies from 0.2a to 0.26a, despite that both the TM-2 and TM-3 bands have slight drops, the large radius of air holes R guarantees the absolute separation, and in turn the bandwidth of single-beam NRR-TM remains at the maximum value when r is smaller than 0.26a. On the other hand, when r increases from 0.26a to 0.35a, the gradually falling TM-3 band causes increasing overlap of the TM-2 and TM-3 bands, so that the single-beam NRR-TM will be reduced, even disappearing when $r = 0.35a$.

To have an overall observation of the dispersion characteristics of such APC systems, the single-beam NRR-TE and single-beam NRR-TM regions for different values of r are summarized in the NRR maps shown in Fig. 5. The corresponding bandwidths of the CNRR occurring in Fig. 5 have also been scanned. Since the single-beam NRR-TE always covers the entire area of single-beam NRR-TM, the behavior of the single-beam NRR-TM is believed to play a critical role in the formation of CNRR. It is clearly seen that when r is chosen within the range 0.13a-0.34a, the APC systems can support the single-beam NRR-TM, and then the single-beam CNRR is available in this situation. In particular, without considering the slight fluctuation on the top of the scanned curve in Fig. 5, the optimum values of r for broad single-beam CNRR will be in the range 0.2a-0.26a, and the corresponding

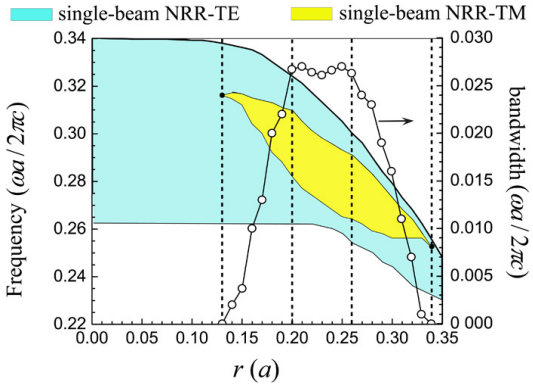

FIG. 5. The single-beam NRR-TE and single-beam NRR-TM areas in APC systems with different values of r when R = 0.47a.

bandwidths are all over 0.026 $2\pi c/a$.

Hence, compared to normal air-hole PCs, such an APC shows more satisfactory dispersion features, which are quite beneficial to the formation of single-beam CNRR. Obviously, such particular dispersion of APCs is attributed to the phase contribution from the extra dielectric rods. When the radius of the dielectric rods is carefully chosen, the APCs can offer complete separation of TM-2 and TM-3 bands and bring substantial overlap between the single-beam NRR-TE and single-beam NRR-TM, which cannot be obtained in normal air-hole PCs.

To find other satisfactory structures of APCs similar to that in Fig. 4, we have also made a survey of the bandwidth of single-beam CNRR for APCs with different values of radii R and r, and Fig. 6(a) shows the corresponding results for several values of R as r changes from 0 to 0.36a. In general, for a particular type of square-lattice 2D PC, the dispersion features of the PC depend largely on the filling factor. A relatively large filling factor in air-hole PCs can push band structures to higher frequencies,

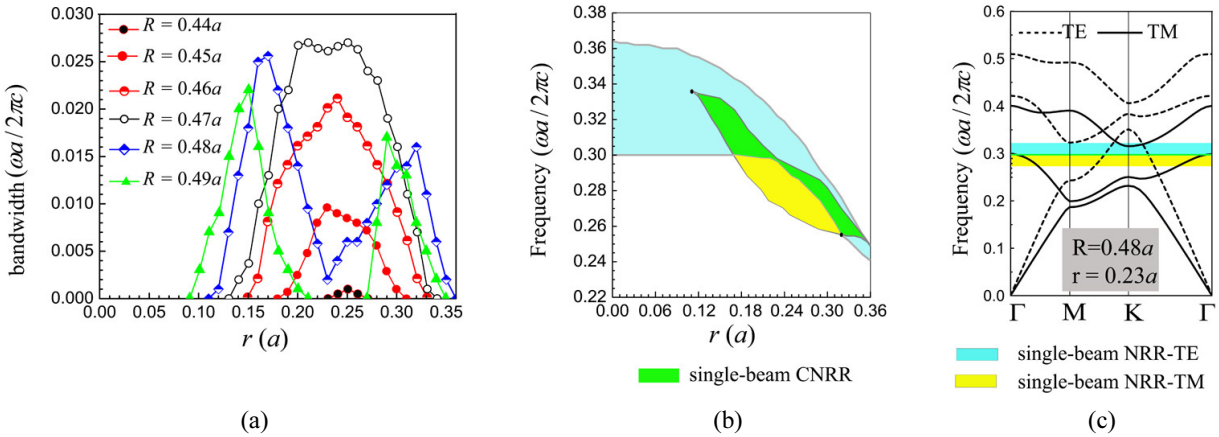

FIG. 6. (a) The bandwidth of single-beam CNRR for an APC, for several values of R as r changes from 0 to 0.36a. (b) The single-beam NRR-TE and single-beam NRR-TM areas in APC systems with different values of r when R = 0.48a. (c) The band structure of an APC with R = 0.48a, r = 0.23a.

while the opposite is true for the case of dielectric-rod PCs. Since the APCs are a combination of these types, which means annular air holes highly favor TE modes while dielectric rods favor TM modes, the single-beam CNRR induced by TE-1 and TM-2 may prefers APCs with relative large radii of both air holes and dielectric rods. As expected, the single-beam CNRR appears when R increases from $0.44a$ and r is no less than $0.1a$. Moreover, as R increases the range of r supporting single-beam CNRR also increases.

On the other hand, when R increases from $0.44a$ to $0.49a$, the scanned curves gradually change from a single peak to double peaks. For cases where R is less than $0.47a$, the curves each have a single peak, and the corresponding peak values increase with the increment of R. However, a slight trough appears on the top of the curve for $R = 0.47a$, and the trough deepens as R continues to grow. Finally, the trough turns into a gap for $R = 0.49a$. To indicate the formation of a trough, Fig. 6(b) shows the NRR map for $R = 0.48a$, and the band structures of an APC with $R = 0.48a$ and $r = 0.23a$ (the corresponding parameters at the bottom of trough) have also been presented in Fig. 6(c). The blue and yellow areas correspond to the single-beam NRR for TE and TM polarizations, respectively. In particular, between the blue and yellow areas there is a partially overlapping region, which is marked by the green area. Comparing Fig. 6(b) to Fig. 5, the single-beam NRR-TM area is almost in the same place, while the single-beam NRR-TE area moves to a higher position when R increases from $0.47a$ to $0.48a$. Additionally, comparing Fig. 6(c) to Fig. 4(b), since the overlapping area between TE-1 and TE-2 becomes larger owing to the increase in R, the single-beam NRR-TE area becomes narrower. As a result, the leaf-like NRR-TM area cannot be fully covered by the NRR-TE area, and a green overlapping area with two peaks appears.

To check the negative-refraction effects, we chose the frequency $0.264\ 2\pi c/a$ as an example to perform numerical simulations of an APC with $R = 0.47a$ and $r = 0.25a$, which are the optimal values of R and r given by Fig. 6(a). Figure 7 shows the calculated EFSs and the corresponding electric-field distributions when a slit beam impinges upon the APC slab with angle of incidence $\theta_{in} = 20°$. It can be clearly seen that the energy flux of the refractive wave follows the negative-refraction law for both polarization waves. In particular, when the incident angle is 20° the refractive angle is calculated to be 5° for TE and 45° for TM, which are in good agreement with estimation from the EFCs in Fig. 7(a). Similarly, in our previous work [14], the negative-refraction effects in an APC with $R = 0.47a$ and $r = 0.188a$ have been studied and verified to separate the polarization beams efficiently. Without providing an exhaustive parameter search, the bandwidth of CNRR in Ref. [14] is about $0.022\ 2\pi c/a$, which is obviously smaller than the optimal bandwidths in this paper. Hence, we believe that other APC structures with optimal parameters

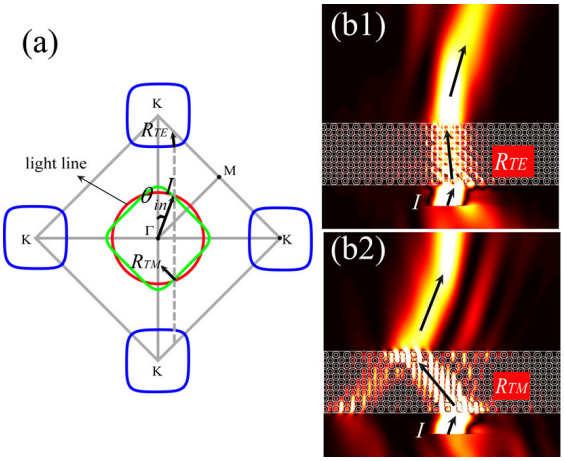

FIG. 7. (a) The EFSs and electric-field distribution when a slit beam impinges upon the APC slab with angle of incidence $\theta_{in} = 20°$ for (b1) TE and (b2) TM. The parameters of the APC are $R = 0.47a$ and $r = 0.25a$. R_{TE} and R_{TM} represent the negative-refracted beams inside the PC slab respectively.

provided in this paper might be used to design polarization beam splitters of wider working bandwidth.

V. SUMMARY

In summary, we have systematically demonstrated the formation of single-beam CNRR between TE-1 and TM-2 in all-dielectric annular photonic crystals with a square lattice. The key physical mechanism of this special effect lies in the fact that band structures of APCs for TM polarization can be pulled down to a lower frequency region, compared to normal air-hole PCs, and APCs with some special filling factors can offer a complete separation of TM-2 and TM-3 bands, which cannot be attained in normal air-hole PCs. These band properties bring a substantial overlap between the single-beam NRR-TE and NRR-TM. Analysis shows that the single-beam CNRR appears when R and r are no less than $0.44a$ and $0.1a$ respectively. Moreover, through an appropriate set of design parameters, the optimal bandwidth of single-beam CNRR can be achieved as over $0.026\ 2\pi c/a$, which is obviously larger than the bandwidth of CNRR used in Ref. [14]. Further numerical results revealed that APC structures with the optimal parameters provided in this paper might be used to design an efficient polarization beam splitter based on the negative-refraction effect, and the wider bandwidth of single-beam CNRR might provide a better-performing polarization beam splitter than that in Ref. [14].

ACKNOWLEDGMENT

This project was supported by the Natural Science Foundation of China (No. 61605087, No. 61704083), the

Natural Science Foundation of Jiangsu Province (No. BK 20160881), the Jiangsu Provincial Natural Science Research Project (No. 16KJB140010) and the Science Foundation of Nanjing University of Posts and Telecommunications (No. NY215064).

REFERENCES

1. V. G. Veselago, "The electrodynamics of substances with simultaneously negative values of ε and μ," Sov. Phys. Usp. **10**, 509-514 (1968).
2. J. B. Pendry, "Negative refraction makes a perfect lens," Phys. Rev. Lett. **85**, 3966-3969 (2000).
3. V. M. Shalaev, "Optical negative-index metamaterials," Nat. Photon. **1**, 41-48 (2007).
4. S. Zhang, W. J. Fan, N. C. Panoiu, K. J. Malloy, R. M. Osgood, and S. R. J. Brueck, "Experimental demonstration of near-infrared negative-index metamaterials," Phys. Rev. Lett. **95**, 137404 (2005).
5. C. Luo, S. G. Johnson, J. D. Joannopoulos, and J. B. Pendry, "All-angle negative refraction without negative effective index," Phys. Rev. B **65**, 201104 (2002).
6. H. L. Ma, B. M. Liang, S. L. Zhuang, J. B. Chen, Q. Jiang, and J. W. Ding, "Subwavelength imaging of a point source based on two-dimensional photonic crystals," Opt. Lett. **41**, 3833-3835 (2016).
7. B. Morvan, A. Tinel, A.-C. Hladky-Hennion, J. Vasseur, and B. Dubus, "Experimental demonstration of the negative refraction of a transverse elastic wave in a two-dimensional solid phononic crystal," Appl. Phys. Lett. **96**, 101905 (2010).
8. P. V. Parimi, W. T. Lu, P. Vodo, J. Sokoloff, J. S. Derov, and S. Sridhar, "Negative refraction and left-handed electromagnetism in microwave photonic crystals," Phys. Rev. Lett. **92**, 127401 (2004).
9. X. D. Zhang, "Absolute negative refraction and imaging of unpolarized electromagnetic waves by two-dimensional photonic crystals," Phys. Rev. B **70**, 205102 (2004).
10. L. Y. Jiang, H. Wu, W. Jia, and X. Y. Li, "Polarization-independent negative refraction effect in SiO_2-GaAs annular photonic crystals," J. Appl. Phys. **111**, 023508 (2012).
11. H. Kurt and D. S. Citrin, "Annular photonic crystals," Opt. Express **13**, 10316-10326 (2005).
12. F. Xia, M. J. Yun, M. L. Liu, J. Liang, W. J. Kong, H. Y. Tan, and W. Lv, "Negative refraction and subwavelength imaging in a hexagonal two-dimensional annular photonic crystal," J. Appl. Phys. **113**, 013109 (2013).
13. P. Shi, K. Huang, X. L. Kang, and Y. P. Li, "Creation of large band gap with anisotropic annular photonic crystal slab structure," Opt. Express **18**, 5221-5228 (2010).
14. H. Wu, L. Y. Jiang, W. Jia, and X. Y. Li, "Polarization beam splitter based on an annular photonic crystal of negative refraction," Chin. Phys. Lett. **29**, 034203 (2012).
15. X. Ao and S. He, "Polarization beam splitters based on a two-dimensional photonic crystal of negative refraction", Opt. Lett. **30**, 2152-2154 (2005).
16. V. Mocella, P. Dardano, L. Moretti, and I. Rendina, "A polarizing beam splitter using negative refraction of photonic crystals," Opt. Express **13**, 7699-7707 (2005).